Automatic Extraction of the Central Symmetry (Mid-Sagittal) Plane from Neuroradiology Images

Yanxi Liu Robert T. Collins

William E. Rothfus, M.D.[a]

CMU-RI-TR-96-40

[a]Associate Professor of Radiologic Sciences, Diagnostic Radiology, Allegheny University of the Health Sciences (Allegheny General Hospital)

The Robotics Institute
Carnegie Mellon University
Pittsburgh, PA 15213

This research is sponsored by the Allegheny-Singer Research Institute under prime contract through the Advanced Technology Program of the National Institute of Standards and Technology (NIST#70NANB5H1183). Views and conclusions contained in this document are those of the authors and should not be interpreted as necessarily representing official policies or endorsements, either expressed or implied, of the National Institute of Standards and Technology or the United States Government.

A shorter version of this work has appeared in SPIE Medical Imaging 1998: Image Processing

Abstract

Normal human brains present an approximate bilateral symmetry. This symmetry is reflected in CT and MR images depicting axial and coronal slices of the brain. Though the internal structure of a pathologic brain may depart from its normal bilateral symmetry, the ideal imaginary bilateral symmetry plane remains invariant. This plane is often referred to as the mid-sagittal plane of the brain. Automatically detecting and explicitly representing the mid-sagittal plane can benefit image understanding in neuroradiology in many ways, including registration, lesion detection, screening and diagnosis. We have developed a simple yet effective algorithm for extracting the axis of bilateral symmetry from each axial brain slice and combining results from multiple slices to determine the central plane of bilateral symmetry for the 3D head. This algorithm has been tested on 12 sets of CT and MR normal and pathological neural scans – a total of 400+ single images. Given a set of axial scans, the accuracy of the algorithm is within one degrees in terms of yaw (< 0.3 degrees) and roll (< 0.75 degrees) angles, and under five pixels in terms of the offset of the symmetry axis. These results are used to correct roll and yaw rotational errors in input images, to automatically produce the midsagittal plane of a given set of axial brain scans, and to detect asymmetries that may be caused by lesions or mass effect in the brain without human intervention.

1 Introduction

Neuroradiology scans are in nature 3D volumetric data expressed as a stack of 2D images. We define an *ideal head coordinate system* centered in the brain with positive X_0, Y_0 and Z_0 axes pointing in the right, anterior and superior directions respectively[1] (Figure 1). With respect to this coordinate system, the *bilateral symmetry plane* of the brain is defined as the plane $X_0 = 0$. This plane is often referred to as the *mid-sagittal* plane of the brain. Ideally, an *axial (coronal)* set of slices are cut perpendicular to the $Z_0(Y_0)$ axis, and their intersection with the bilateral symmetry plane (mid-sagittal plane) is a vertical line on each slice. In clinical practice, due to various positioning errors, we are presented not with the ideal coordinate system, but rather a *working coordinate system* XYZ in which X and Y are oriented with the rows and columns of each axial image slice and Z is the actual axis of the scan (Figure 1). The orientation of the working coordinate system differs from the ideal coordinate system by three rotation angles, *pitch, roll* and *yaw*, about the X_0, Y_0 and Z_0 axes, respectively.

Normal human brains present an approximate bilateral symmetry. This symmetry is reflected in CT and MR images depicting axial and coronal slices of the brain. Indeed, neuroradiologists often refer to asymmetries of the brain in these images as an indicator of a possible abnormality (Figure 2). Such asymmetries are caused either by *mass effect,* which is the displacement of normal anatomical structures away from their normal positions, or by a density imbalance due to a tumor or bleed etc. in or around the brain.

Although the internal structure of a pathologic brain may depart from its normal bilateral symmetry, the ideal imaginary bilateral symmetry plane remains invariant. Automatically detecting and explicitly representing the bilateral symmetry plane of the brain can benefit image understanding in neuroradiology in many ways:

- **registration:** the bilateral symmetry plane provides a common plane for aligning different sets of normal or pathological 3D brain images;
- **screening:** asymmetries in an axial (coronal) slice (with respect to its ideal bilateral symmetry plane) provide a basis for visually screening brain scans for pathological cases;
- **detection:** the symmetry axis on each brain slice provides a center line for detecting bilateral asymmetries such as mass effects and lesions;
- **diagnosis:** classification of a lesion is invariant under reflection about the mid-sagittal plane.

[1] This definition is similar to the one defined in the Talairach Brain Atlas [10] except for the pitch angle.

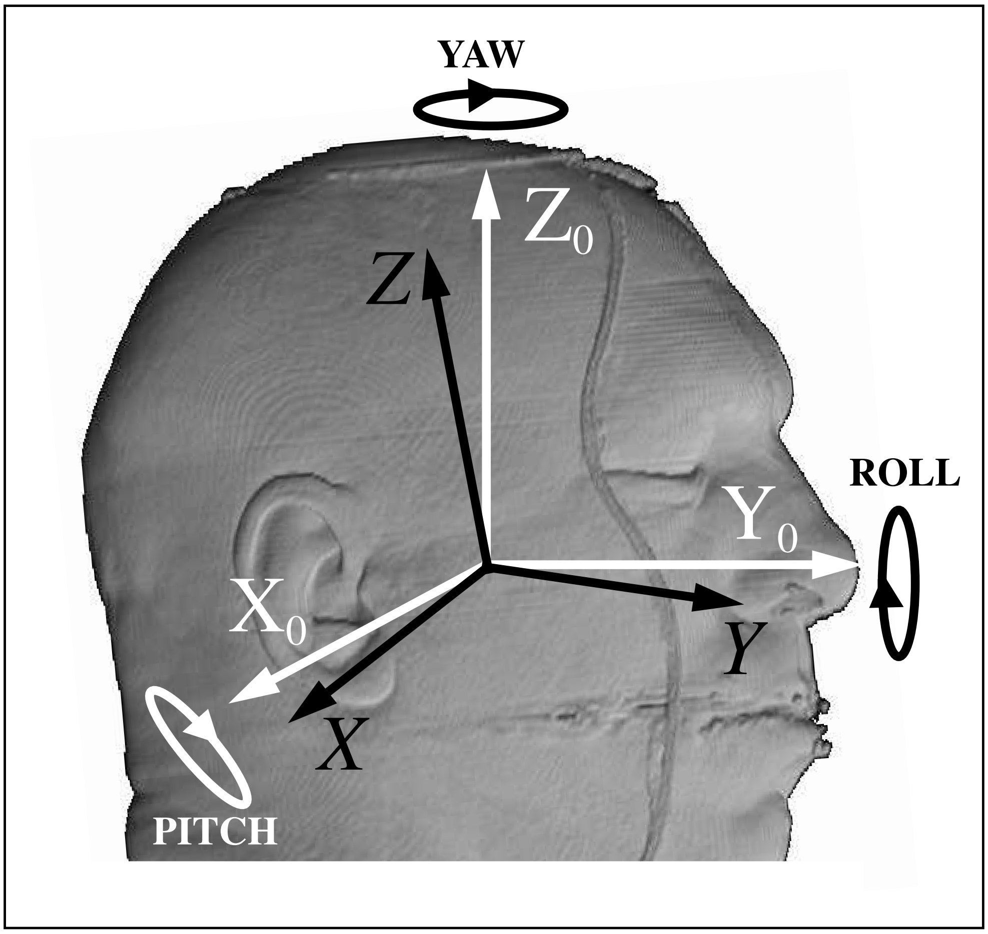

Figure 1: Ideal head coordinate system $X_0Y_0Z_0$ vs. the working coordinate system XYZ. Rendered head courtesy of the Visible Human Project.

Our long term goal is to build a content-based neuroradiology image understanding system that can intelligently store, retrieve and compare images. We believe that an understanding of brain symmetry is crucial to the success of this effort.

From a given set of axial (coronal) CT or MR brain slices, it is non-trivial to capture the mid-sagittal plane automatically since

- there is no enforced standard among technicians when taking brain scans. Each set of slices may differ from other sets in the angle of scanning (pitch), the start or end positions of the scan, the distance between adjacent slices, and the total number of slices;
- the patient's head may be tilted during the scanning process, resulting in an off-centered set of slices with non-zero yaw and roll angles;
- the human skull and brain are only approximately symmetric – asymmetries such as air pockets and the presence of lesions must be ignored when computing the axis of symmetry.

We have developed a simple algorithm that can extract the axis of bilateral symmetry of a brain slice from an axial (coronal) CT or MR image regardless of background clutter, asymmetries of the skull, or the presence of mass effect and brain pathologies such as tumors, bleeds or stroke (Sections 2.1 and 2.2). Axes from multiple slices are combined in an optimization process to produce a best fit bilateral symmetry plane for the 3D volume of images, along with an estimate of the yaw and roll rotation angles of the head (Section 2.3), and the extraction of the mid-sagittal plane. These results are applied to the detection of asymmetries in the slices, which may be caused by lesions or mass effect in the brain (Section 3). This algorithm differs from [1], and other window-based methods which work on MR images of brains *without major anatomical distortion*, and uses no preset fiducial markers placed on the patient.

2 Bilateral Symmetry Analysis

The input to our bilateral symmetry analysis procedure is a set of CT or MR images from an axial (coronal or sagittal) brain scan, along with metric data reporting pixel dimensions and the distances between adjacent slices (Figure 2). Given this data, the algorithm automatically determines the central plane of reflectional symmetry passing through the middle of the brain, and measures the roll and yaw rotation angles of the 3D scan with respect to the ideal head coordinate system shown in Figure 1. The process is decomposed into the following steps:

1. isolate the head region from background clutter on each slice;
2. extract the 2D axis of reflectional symmetry from each slice;

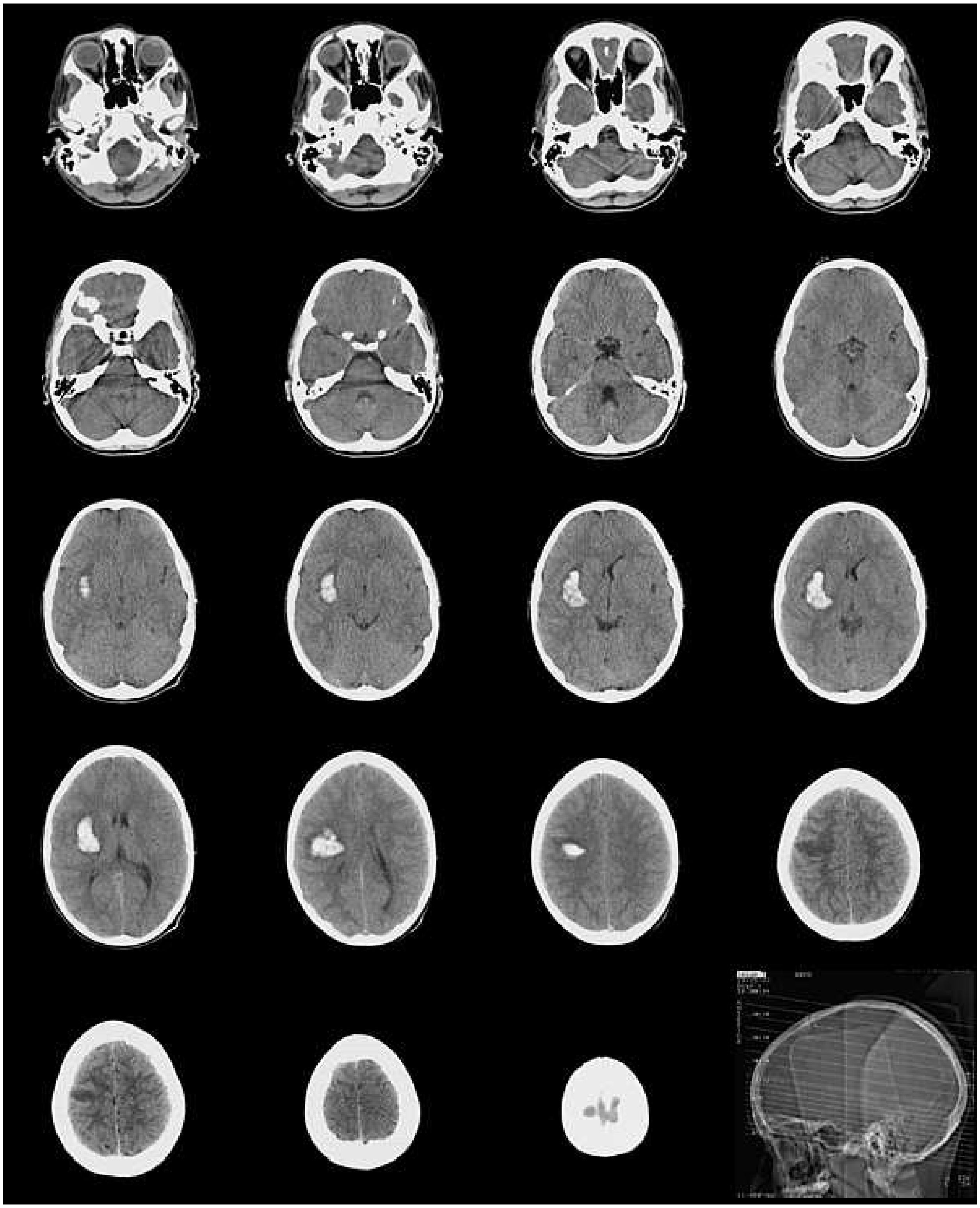

Figure 2: A set of input axial CT scans. This is a case of acute right basal ganglion bleed.

3. combine symmetry axis results from all slices to estimate a best-fit plane of reflectional symmetry for the 3D volume;
4. compute the roll and yaw angles of the scan.

2.1 Isolating the Head Region

A typical brain scan is dominated by the patient's head shown against a dark background, but sometimes there is also clutter in the form of patient data and acquisition parameters superimposed on the slice, as well as the physical cross-section of the headrest that is holding the patient's head steady (see Figure 3a). We have developed a simple procedure for preprocessing each slice to remove this clutter and thereby isolate just the head region.

We first binarize the image by assuming that the first prominent peak in an intensity histogram of the slice corresponds to the dark background pixels. We choose a threshold to the right of this peak by first smoothing the histogram, computing the second derivative of the smoothed histogram curve, then choosing the second zero-crossing of the second derivative (which corresponds to the the point of inflection of the descending side of the first peak) as the position of the grey value threshold T. This threshold is used to binarize the slice by setting all pixels with intensity lower than T to zero, and all other pixels to one (Figure 3b).

The binary image formed in this way is segmented into separate regions by grouping together one-pixels into four-connected components. Assuming the head is the dominant structure in the image, the region containing the largest number of pixels is considered to represent the head, and all others are discarded by setting their pixel values to zero. Any holes in the head region (corresponding to dark areas on the slice caused by air in the sinuses or ear canals) are detected and filled in, resulting in a binary mask with one-pixels representing the patient's head, and zero-pixels representing the background and discarded clutter (Figure 3c). This mask is then multiplied pointwise with the original greyscale slice image to produce a new grey-level image showing just the head (Figure 3d). This is the image used by the rest of the system for rotation analysis and lesion detection.

This preprocessing procedure has been tested on a large number of slices and has proven to be very effective in isolating the main head region on the slice. Many times, thin structures that are technically part of the patient's head, such as skin or ear cartilage, are cropped off with this technique, but these are not important for our application. The only time we have observed this method to fail is on an unusual set of slices that contain cloudy-looking, extraneous densities in the background, some of which gets included with the head region in the final image. However, since the head region was still completely included in the final images, even this failure did not have a

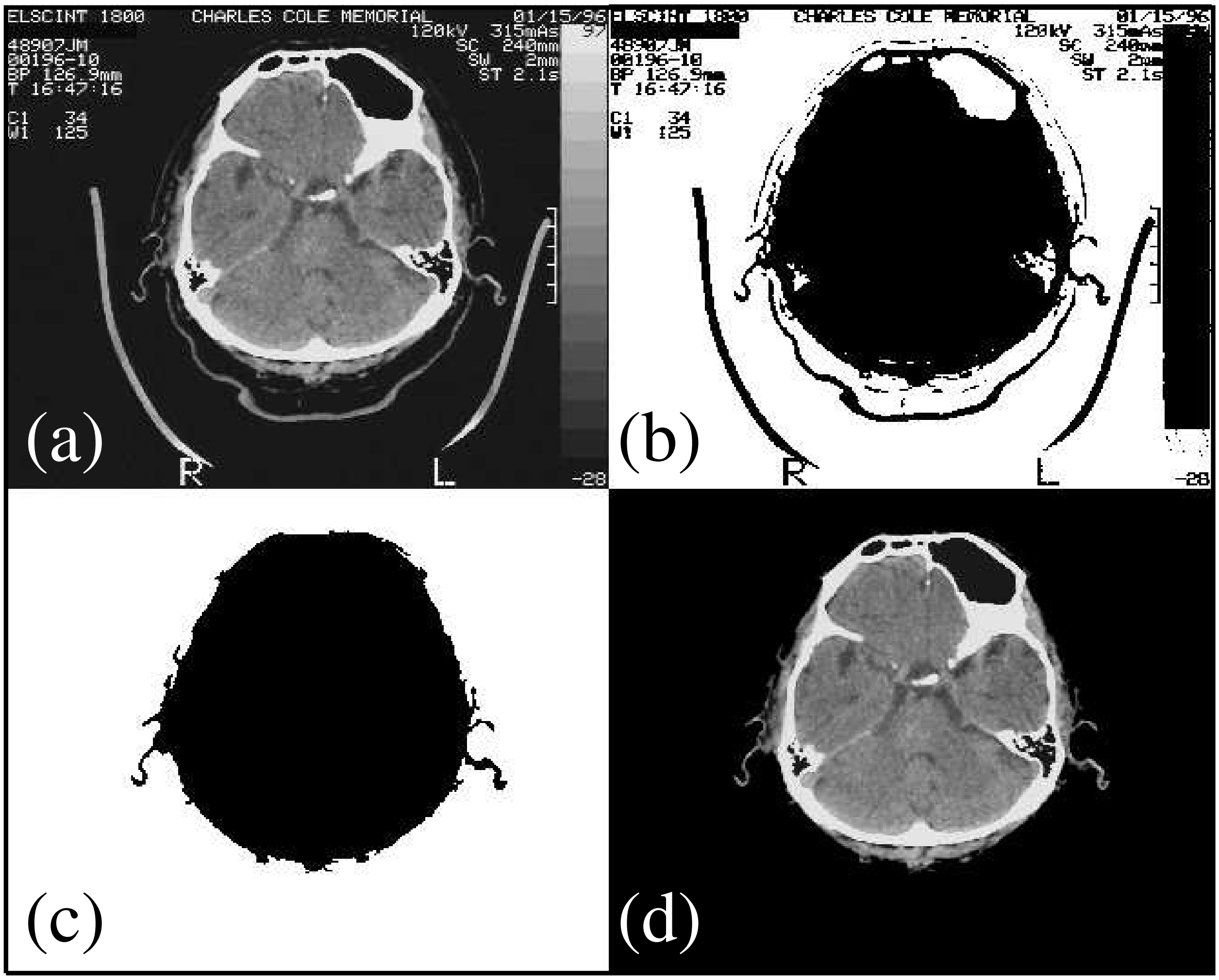

Figure 3: Isolating the Head Region

detrimental effect on the rest of the system.

2.2 Symmetry Axis Extraction

Under the *working coordinate system,* the central symmetry plane is represented as

$$aX + bY + cZ + d = 0, \tag{1}$$

and the ith slice is on the plane $Z = Z_i$. The symmetry axis (a 2D line) on the ith slice is the intersection of the above two planes:

$$aX + bY + (cZ_i + d) = 0. \tag{2}$$

From this equation, we can see immediately that the orientation angle θ_i of the 2D symmetry axis, namely $\theta_i = \arctan(b/a)$, should be the same for all slices regardless of their Z_is. This is actually the yaw angle of the bilateral symmetry plane (see Section 2.5).

We first estimate the orientation of the symmetry axis of each slice. To estimate the 2D symmetry axis of image S_i, representing slice $Z = Z_i$, we refer to the definition of bilateral symmetry: a reflection of image S_i about its symmetry axis produces a figure S_i' that is approximately identical to S_i. We thus search for the orientation of the reflection line that maximizes the cross-correlation between the original image and the rotated, reflected image. First the image S_i (Figure 4a) is reflected about its vertical center line, to produce a new image $ref_V(S_i)$ (Figure 4b). If the reflection axis of S_i is oriented θ degrees from vertical, then the symmetry axis of $ref_V(S_i)$ will be oriented $-\theta$ degrees from vertical. Thus $ref_V(S_i)$ would have to be rotated by 2θ degrees for it to have the best 2D cross-correlation score with S_i (the maximum of the 2D cross-correlation surface is chosen as the correlation score at a given angle, yielding the best correlation results for any relative translation of S_i with respect to $rot(2\theta, ref_V(S_i))$.

To search for the best orientation θ, we rotate $ref_V(S_i)$ about the center of the image, cross-correlate with the original image S_i, and record the maximum correlation value $C_i(\theta_j)$ for each θ_j (Figure 5a). In most instances a single, well-defined peak results, especially for the lower brain slices. This is because the slices lower in the brain present complex bilateral bony structures in contrast to the slices higher in the brain, which become ovals or even near-circular at the tip of the head.

The actual search is performed in frequency space[2], for efficiency. That is,

$$C_i(\theta_j) \quad = \quad \max \{ \text{XCorr}(S_i, rot(2\theta_j, ref_V(S_i)) \}$$

[2]Note that since the Fourier transform $\mathcal{F}$ commutes with rotations and vertical reflections, we only have to compute the Fourier transformation of S_i once – the flipped and rotated versions can be generated directly in frequency space by flipping and rotating the image $\mathcal{F}(S_i)$.

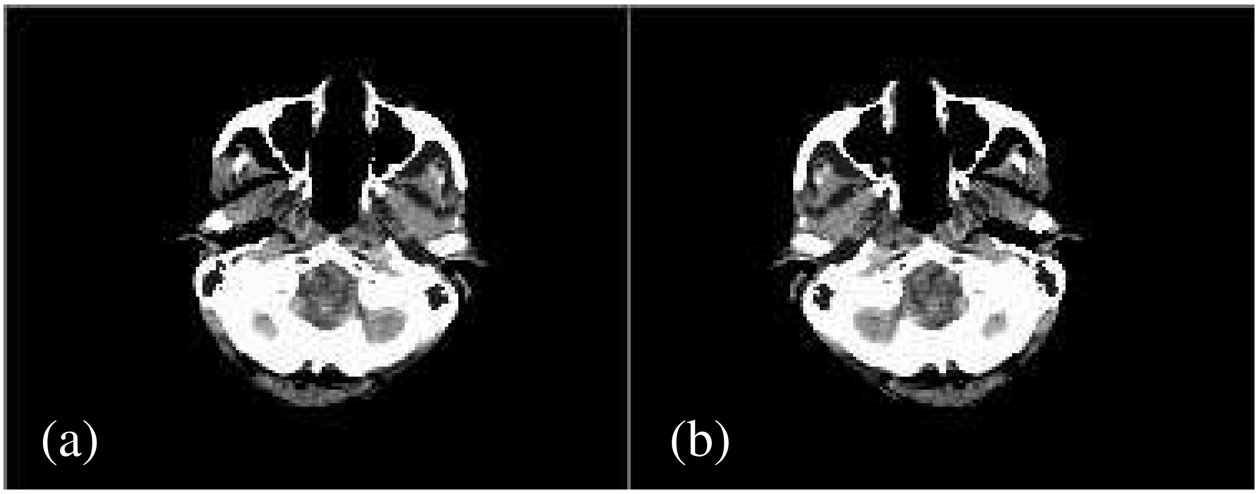

Figure 4: a) A CT axial Head image S_i. b) Vertically reflected image $ref_V(S_i)$.

$$= \max \left\{ \mathcal{F}^{-1}(\mathcal{F}^*(S_i) rot(2\theta_j, ref_V(\mathcal{F}(S_i)))) \right\}.$$

where $\mathcal{F}^*(S_i)$ is the complex conjugate of Fourier transform of S_i and F^{-1} is the inverse Fourier transformation [8, 9].

Since all brain slices in the scan should have the same symmetry axis orientation (Equation (2)), we combine results from each slice to produce a cumulative result. This is done by adding all the cross-correlation curves C_i from different slices $C(\theta_j) = \Sigma C_i(\theta_j)$, smoothing the curve with a Gaussian filter, and finding the index θ_{max} of the peak of the smoothed curve. Figure 6 shows a plot of the summed correlation values C vs. possible orientation angles θ_j. The final estimate of the symmetry axis orientation for the set of brain slices is the angle θ_{max} such that the maximum correlation value max$(C) = C(\theta_{max})$. For the set of CT slices containing the image in Figure 4, the maximum value of the fitted curve to $C(\theta_j)$ on Figure 6 is -6.5 degrees.

After the best orientation θ_{max} has been decided for the set of scans, we compute the offset $trans_i$ of the symmetry axis in each image. We first rotate each image S_i by angle $-\theta_{max}$ so that its symmetry axis is oriented vertically. We then cross-correlate that image with a vertical reflection of itself about the center of the image. The column at which the two produce the highest correlation value is chosen as the value of $trans_i$ for that slice.

2.3 Central Symmetry Plane Fit

At the end of the above procedure, we have obtained a set of parallel symmetry axes for the set of images. All symmetry axes share a common orientation θ_{max} and each of them has an individual estimate of translation $trans_i$. From Equation (2) and Figure 7, the offsets $trans_i$ of the symmetry

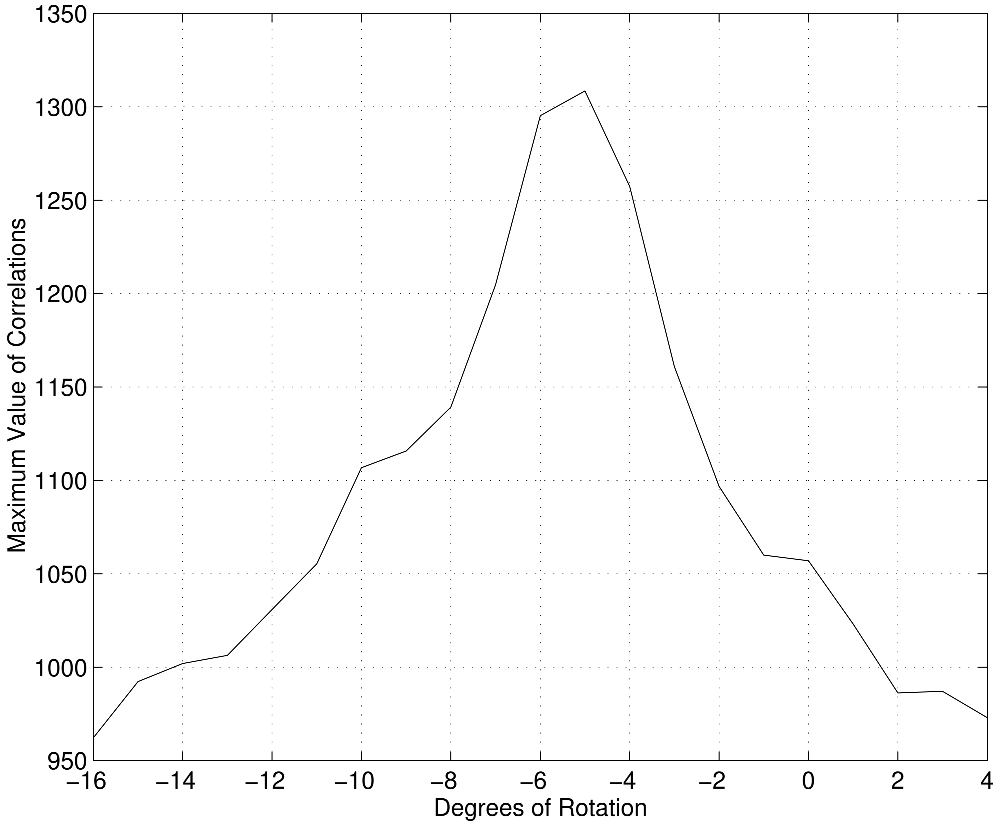

Figure 5: Plot of the maximum cross-correlation between $rot(2\theta_j, ref_V(S))$ and S, for θ_j between -16 and 4 degrees sampled at every 1 degree.

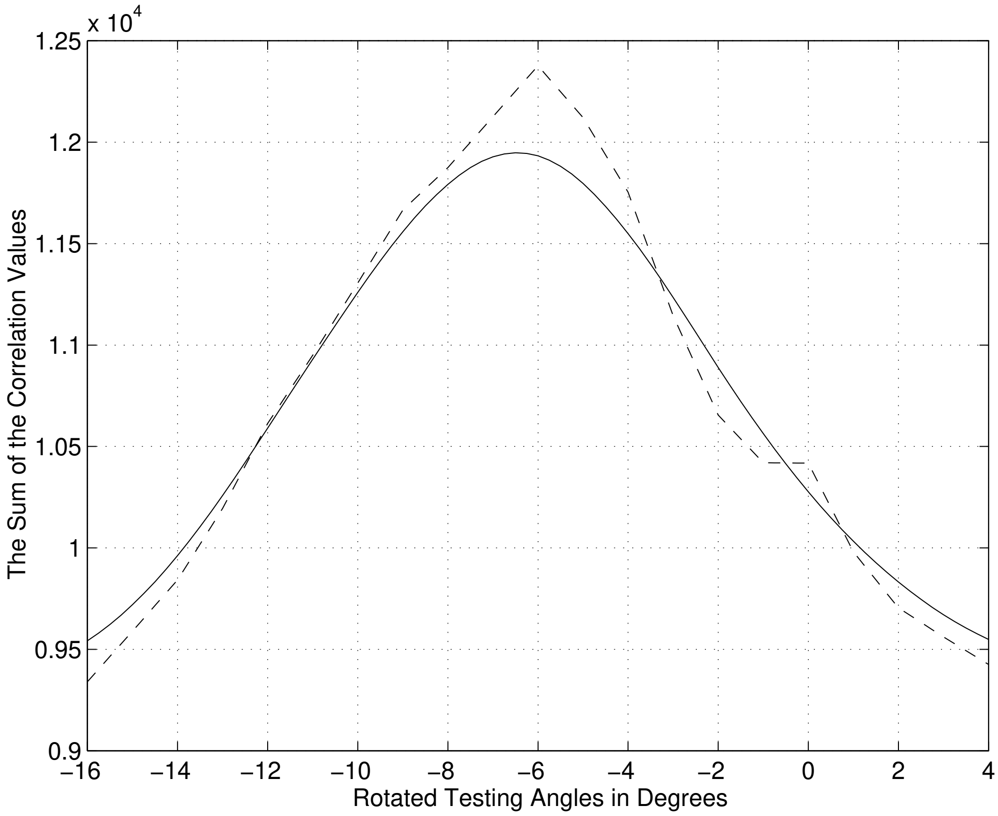

Figure 6: The dashed line is the sum of all the cross-correlation plots, $C(\theta_j) = \Sigma C_i(\theta_j)$ when θ_j changes from -16 to 4 degree. The solid line is the curve after Gaussian smoothing.

axis of each slice $Z = Z_i$, though they may vary from slice to slice, have a simple linear relationship with Z_i:

$$trans_i = cZ_i + d \ . \tag{3}$$

This relationship, taken over all slices, forms a linear set of equations that we use to compute optimal values for c and d. The parameters c and d, together with the parameters $a = \cos\theta_{max}$ and $b = \sin\theta_{max}$ complete our estimation of the symmetry plane equation (1). As a final step, we recompute an optimized symmetry axis on each slice, with an orientation of θ_{max} and an offset final_trans$(i) = c * Z_i + d$. This is equivalent to intersecting the estimated symmetry plane with each brain slice to obtain a new set of 2D symmetry axes.

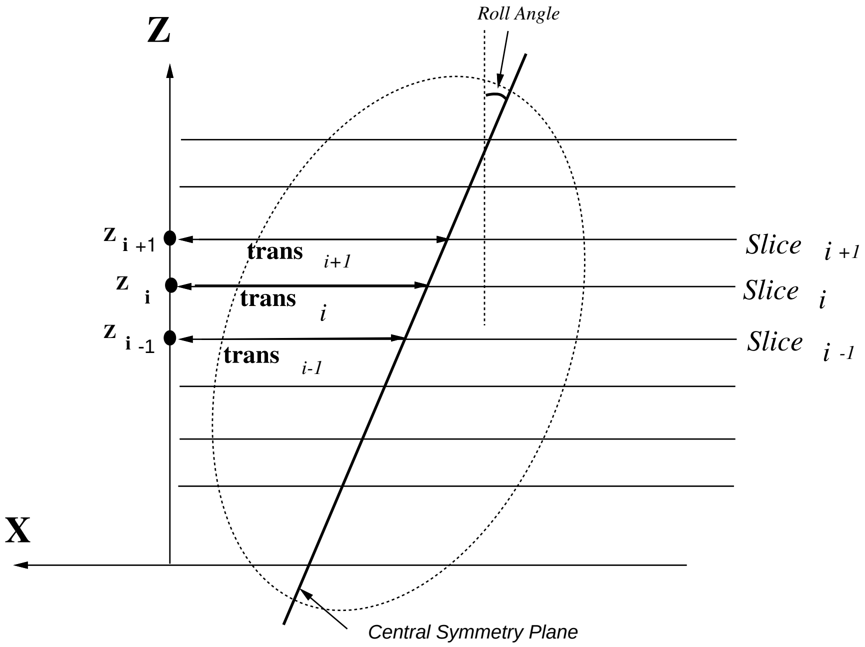

Figure 7: The relationship between the symmetry axis offset $trans_i$ and brain slice i's position along the Z axis Z_i

2.4 Results

The algorithm has been tested on 9 sets of CT and 3 sets of MR images. The CT scans are rectangular 8-bit density images with an average size of 630 $\times$ 550, and an average number of slices per set of 20. MR image sizes are around 240 $\times$ 180, and the numbers of slices in each set varies from 30 to 200. The estimated symmetry axes extracted by our algorithm are located within a few pixels of the ideal axes picked by hand. In the following we show some samples of our results. For a more complete set of results, access the web site: http://www.cs.cmu.edu/∼yanxi/www/home.html and follow the link to medical imaging.

Figure 8 shows the final symmetry axis extracted on each input brain slice from Figure 2.

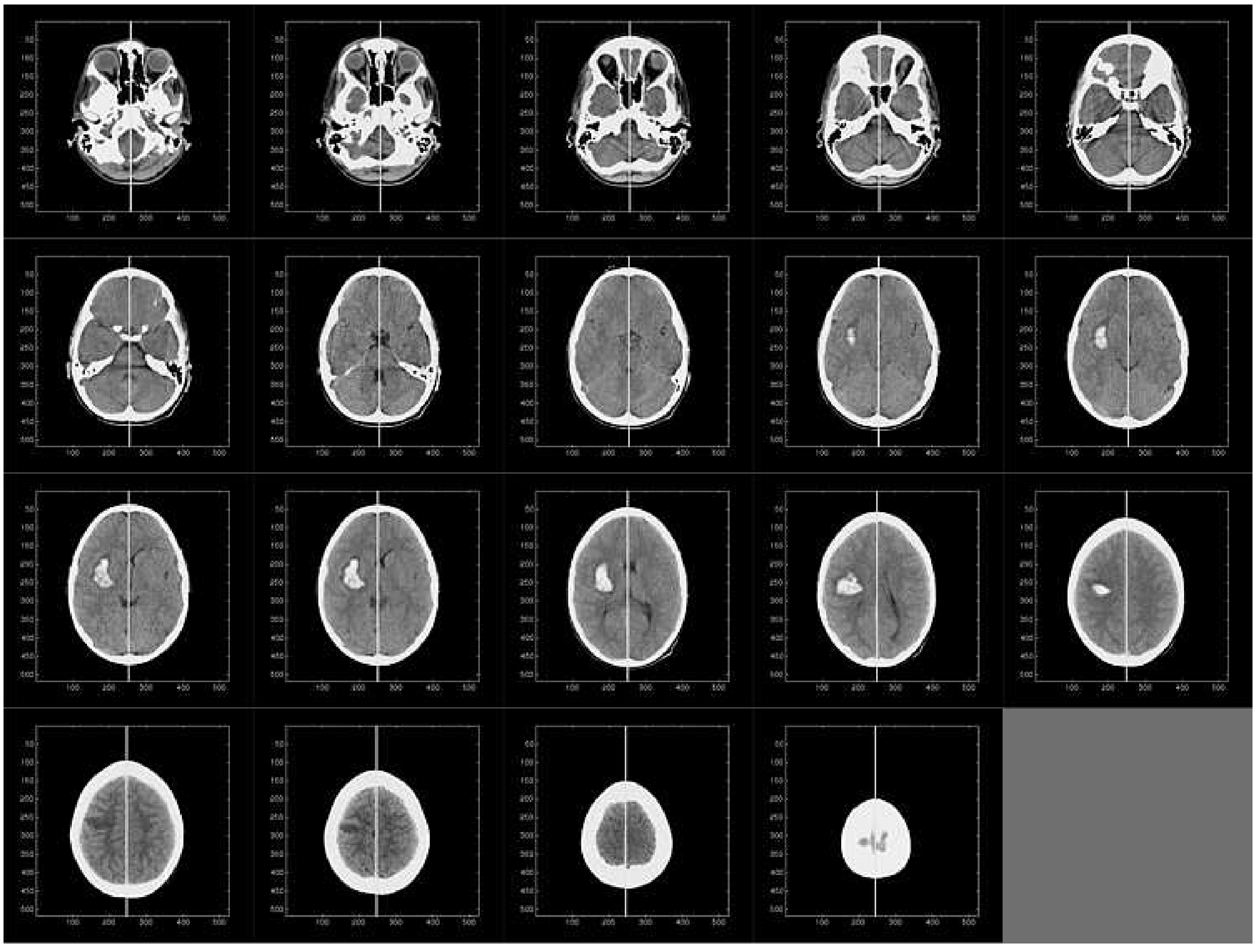

Figure 8: Final symmetry axes superimposed on a set of CT scan slices.

Figure 9 shows the plot of X offset of the symmetry axis on each CT slice shown in Figure 8 before and after fitting the central symmetry plane to the individually computed symmetry axis. Figure 10 shows a similar plot for a set of 187 MR slices. Notice the MR example shows an almost vertically fitted symmetry plane given the input data (the $trans_i$ value difference between top and bottom axial slices, nearly 200 slices, is only 4 pixels or about 3.9mm) while the CT example displays an extracted symmetry plane with a relatively large span of $trans_i$ values (the difference in $trans_i$ between the top and the bottom slices is 13 pixels which is about 6.5mm) indicating a larger roll angle in the input axial slices.

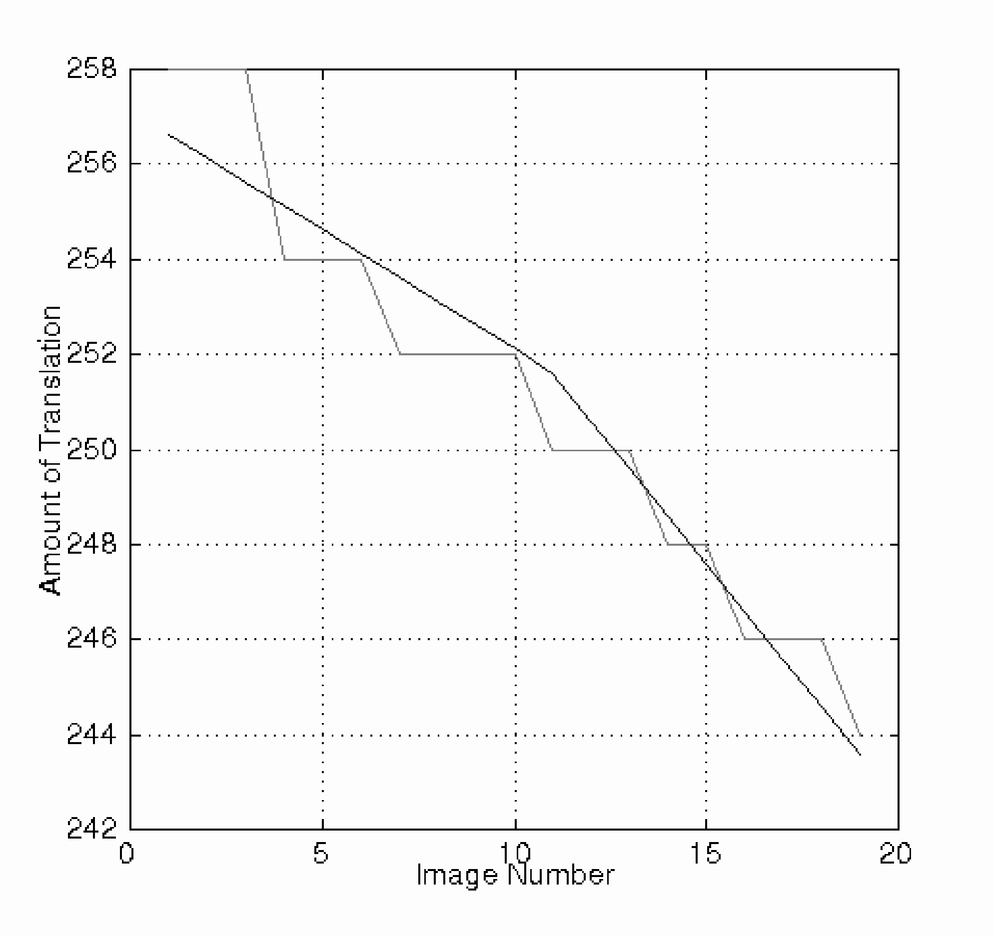

Figure 9: The fitted central symmetry plane is superimposed on top of the offset $trans_i$ computed for the symmetry axis on each CT scan. The pixel dimensions are 0.5×0.5mm, the first 11 slices have spacing 5mm and the last 8 slices have spacing 10mm. Horizontal axis is the brain slice index, with lower numbers corresponding to lower cuts. Vertical axis is the amount of offset (translation) of the symmetry axes in pixels. The bending is due to a change of slice spacing from 5 to 10 mm. The calculated roll angle is 2.87 degrees.

Figures 11, 12 and 13 show the extracted symmetry axes under various conditions, note the symmetry axes are not affected by the pathological cases and mass effects in the images.

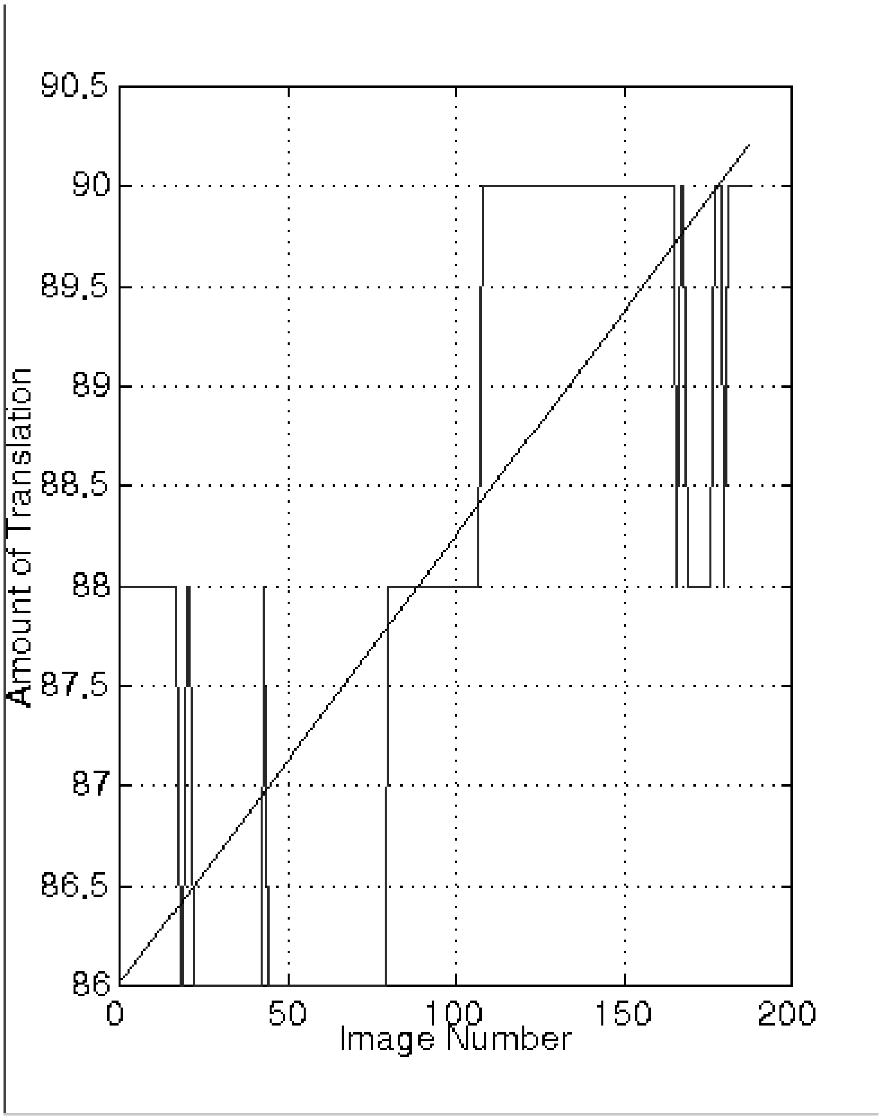

Figure 10: Plot of the central symmetry plane fitted to the offsets of the symmetry axes extracted from a set of MR images: volume $176 \times 236 \times 187$ with voxel size $0.98 \times 0.98 \times 1.2$mm. Horizontal axis is labeled in terms of the brain slice index and vertical axis is in pixels. The detected roll angle is -1.75 degrees.

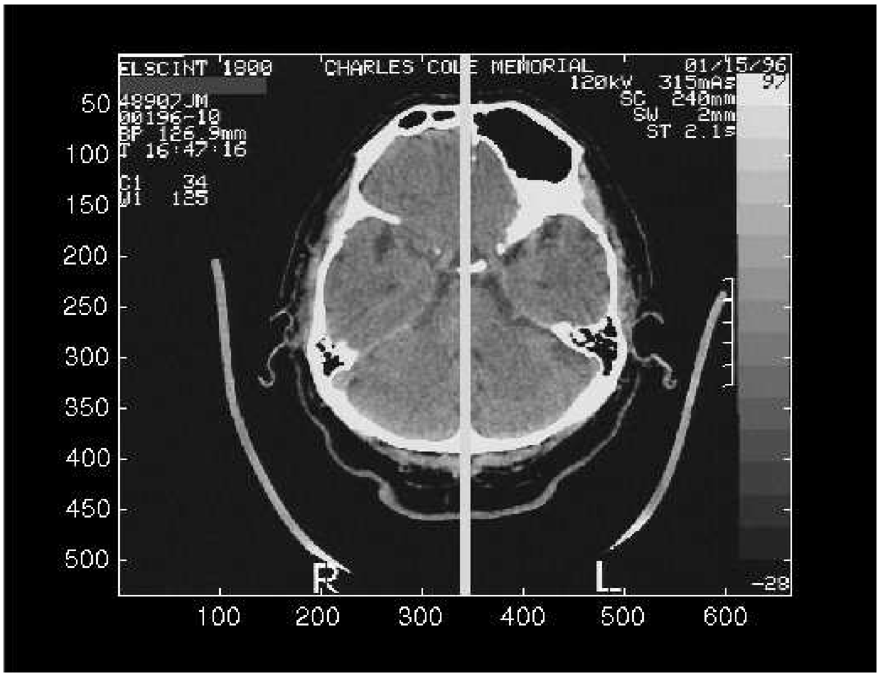

Figure 11: The symmetry axis extracted from a CT scan where obvious asymmetry is present due to a dilated frontal sinus outside of the brain.

2.5 Computing Roll and Yaw Angles

By now, we have completely determined the geometric equation $aX + bY + cZ + d$ of the central symmetry plane with respect to the working coordinate system, where (a, b, c) is a unit normal to the plane and d is its distance from the origin. At this point, we are ready to estimate the orientation of the working coordinate system with respect to the ideal head coordinate system by computing the roll, yaw and pitch rotation angles that bring their axes into alignment.

Under the ideal coordinate system, the orientation of the bilateral symmetry plane is $(1, 0, 0)$. Due to tilting of the patient's head, and an arbitrary decision by the technician as to the pitch angle, points in the ideal coordinate system are reoriented into the observed working coordinate system by an unknown general rotation

$$\begin{aligned}\mathcal{R} &= \mathbf{yaw}(\theta)\mathbf{roll}(\phi)\mathbf{pitch}(\omega) \\ &= \begin{bmatrix} c\phi\, c\theta & c\theta\, s\omega\, s\phi - c\omega\, s\theta & c\omega\, c\theta\, s\phi + s\omega\, s\theta \\ c\phi\, s\theta & c\omega\, c\theta + s\omega\, s\phi\, s\theta & c\omega\, s\phi\, s\theta - c\theta\, s\omega \\ -s\phi & c\phi\, s\omega & c\omega\, c\phi \end{bmatrix}\end{aligned}$$

where $c\theta \equiv \cos\theta$, $s\theta \equiv \sin\theta$, and so on. This rotation transforms the unit normal of the symmetry

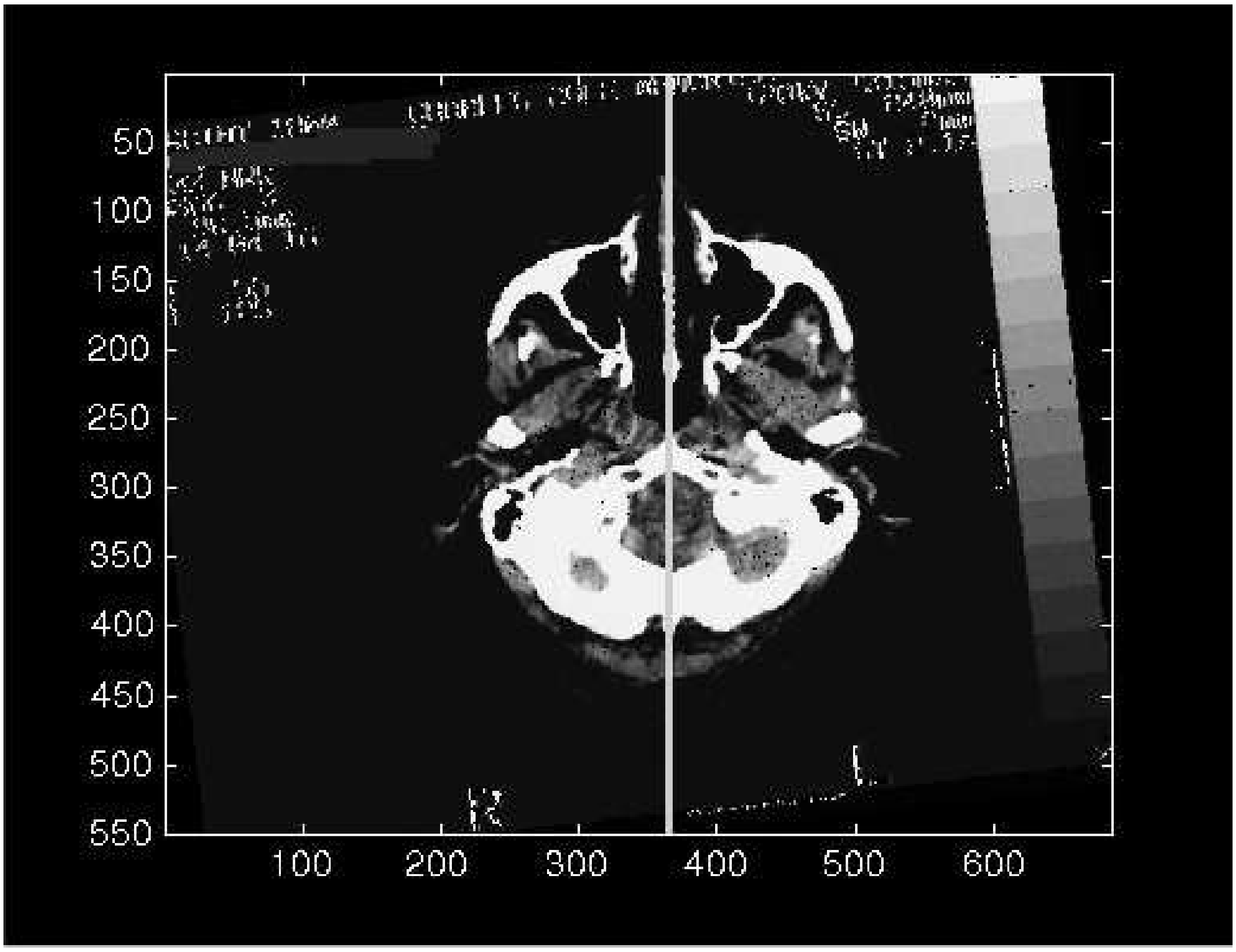

Figure 12: The symmetry axis is extracted and the image is rotated to correct the yaw angle error (-6.5 degree) in the input data.

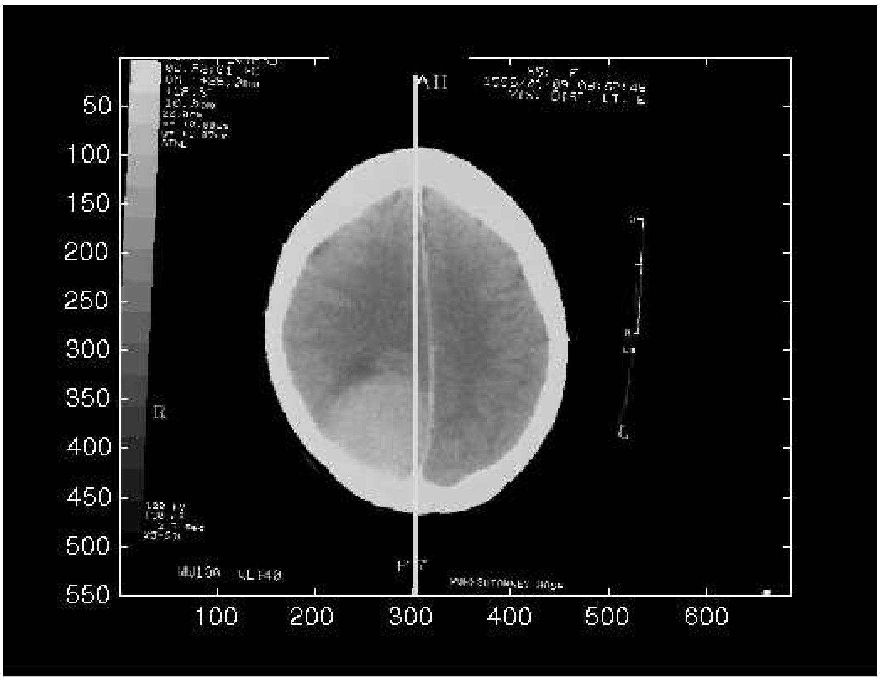

Figure 13: The symmetry axis extracted from a CT scan where obvious asymmetry is present due to a tumor.

plane from $(1, 0, 0)$ to

$$\mathcal{R}(1, 0, 0)^T = (\cos\phi \, \cos\theta, \cos\phi \, \sin\theta, -\sin\phi)^T.$$

Thus, the symmetry plane equation can be rewritten in terms of its yaw and roll angles

$$\cos\phi \, \cos\theta X + \cos\phi \, \sin\theta Y - \sin\phi Z + d = 0$$

Matching up our plane parameters a, b, c (Equation (1)) with this equation, we find by inspection that

$$\tan\theta = b/a$$
$$\tan\phi = -c/\sqrt{(a^2 + b^2)} \tag{4}$$

from which we can easily compute the roll angle ϕ given the input as axial slices, or compute the yaw angle θ given the input as coronal slices. We call the angle obtained directly by image correlations as *detected* angle value, and the angle obtained by using Equation (4) as *calculated* angle value.

To test our algorithm, the input MR image set was resampled using trilinear interpolation to artificially vary the yaw angles from -10 to 10 degrees in 2.5 degree intervals, and the roll angles from -15 to 15 degrees in 5 degrees intervals. Table 1 shows the result of detected yaw angles and computed roll angles given a set of axial slices with varied yaw angles. Table 2 shows the result of detected roll angles and computed yaw angles given a set of coronal slices with varying roll angles (Figure 14). The average accuracy of the algorithm on both yaw and roll angle detection is under

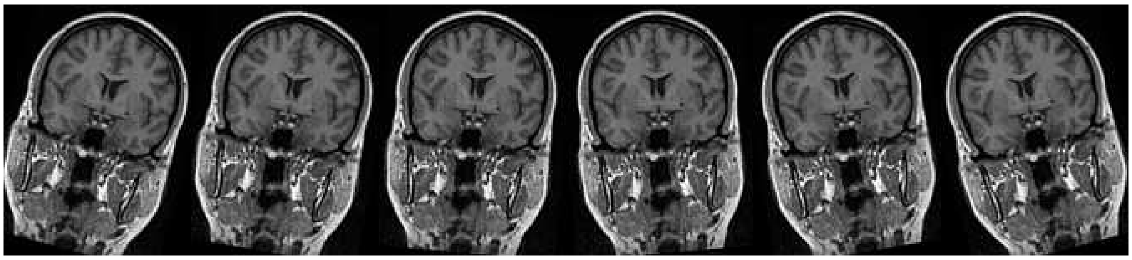

Figure 14: One slice sample from the coronal input with varied roll angles.

one degree (< 0.3 degrees for the yaw angles and < 0.75 degrees for the roll angles), after taking into account the nonzero yaw angle of 1.25 degrees and roll angle of -1.75 in the original dataset (Figure 15, Figure 16). Given the sample interval for finding the symmetry axis on each slice is one degree, this result is optimal.

Table 1: Numerical Results When Varying the Yaw Angle

Yaw Angle	-10	-7.5	-5	-2.5	0	2.5	5	7.5	10
Detected Yaw Angle	-8.5	-5.75	-3	-0.5	**1.25**	4.0	6.5	8.75	11.25
Calculated Roll Angle	-1.4	-1.7	-1.3	-1.4	-1.29	-1.7	-1.7	-1.3	-1.3

Table 2: Numerical Results When Varying The Roll Angle

Roll Angle	-15	-10	-5	0	5	10	15
Detected Roll Angle	-17	-12	-6.75	**-1.75**	2.75	7.75	12.5
Calculated Yaw Angle	0.5	0.3	2.7	0.7	-0.07	0.34	0.8

Given a volumetric data, our algorithm can identify the errors in yaw and roll angles in the input data, and correct these errors by recutting the input volume. See Figure 17 for a comparison of the original input axial slices with the corresponding recut slices after correcting the detected yaw and roll angles (yaw angle $= 2.5$ degrees and the roll angle $= 2.87$ degrees)in the input volumetric data. Notice the recut slices are more visually symmetric than the input slices.

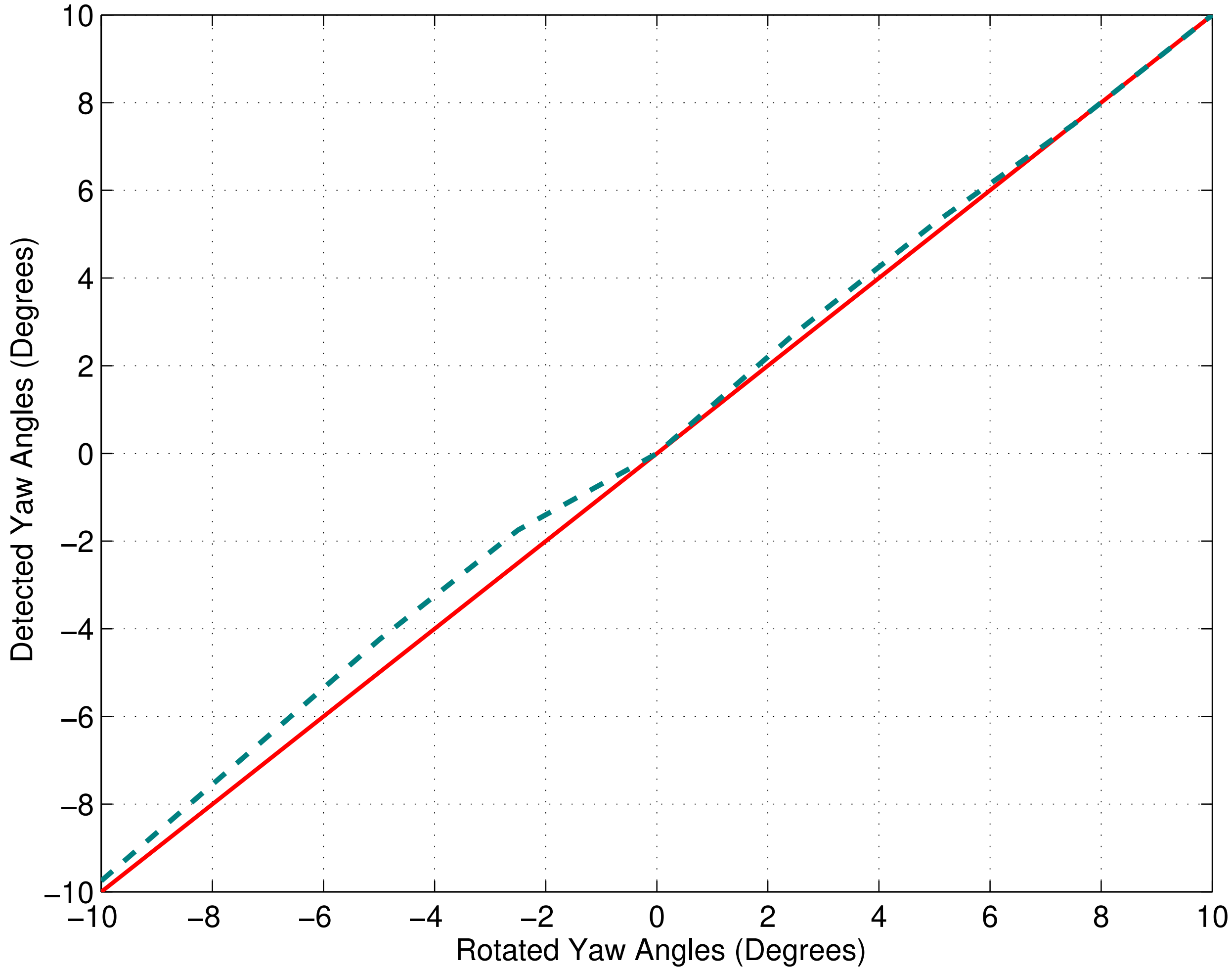

Figure 15: Actual vs detected yaw angles in the MR original axial scans. The solid line is the perfect detection result and the dashed line is formed from the detected yaw angle values using our algorithm.

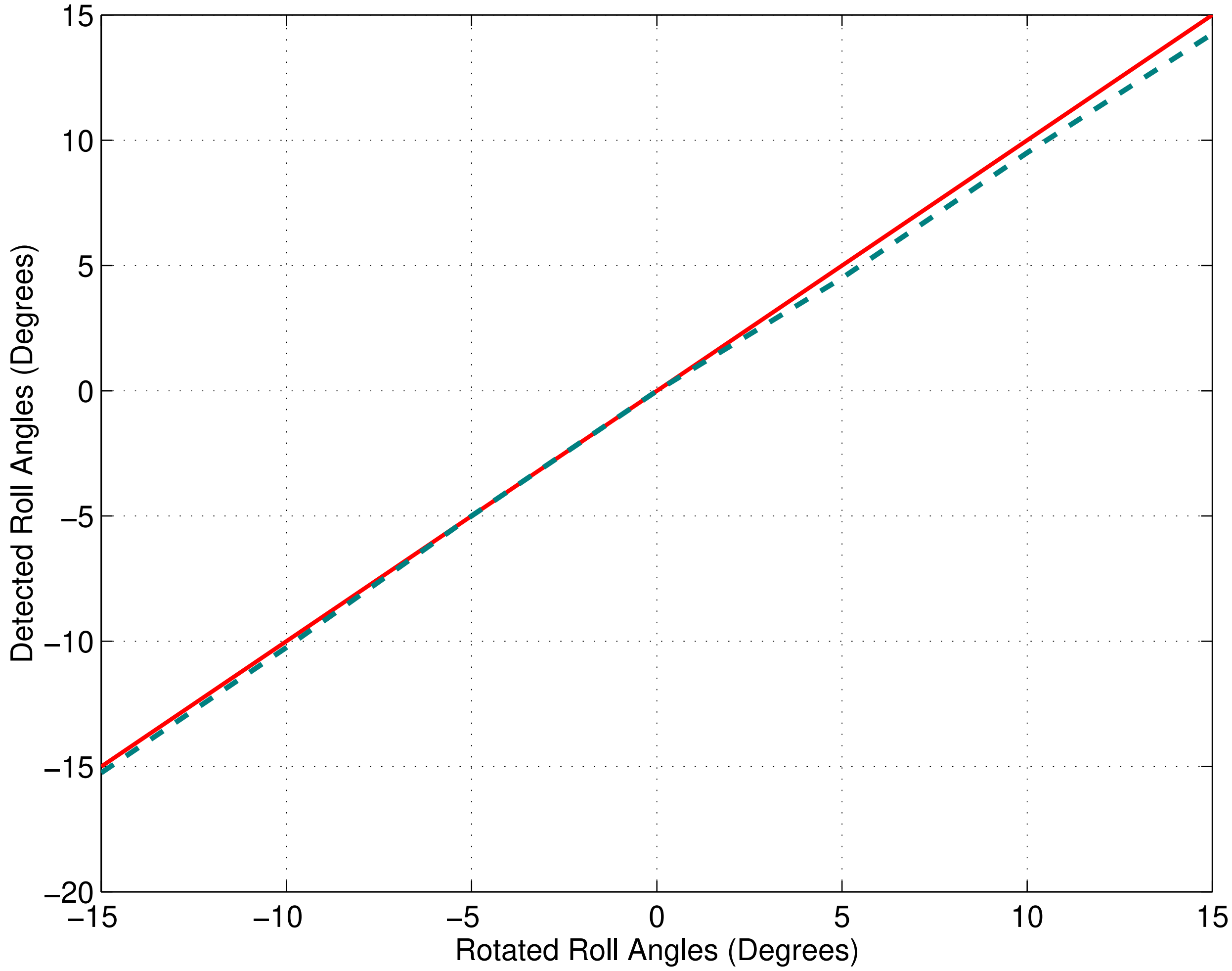

Figure 16: Actual vs detected roll angles in the MR resliced coronal scans. The solid line is the perfect detection result and the dashed line is formed from the detected roll angle values using our algorithm.

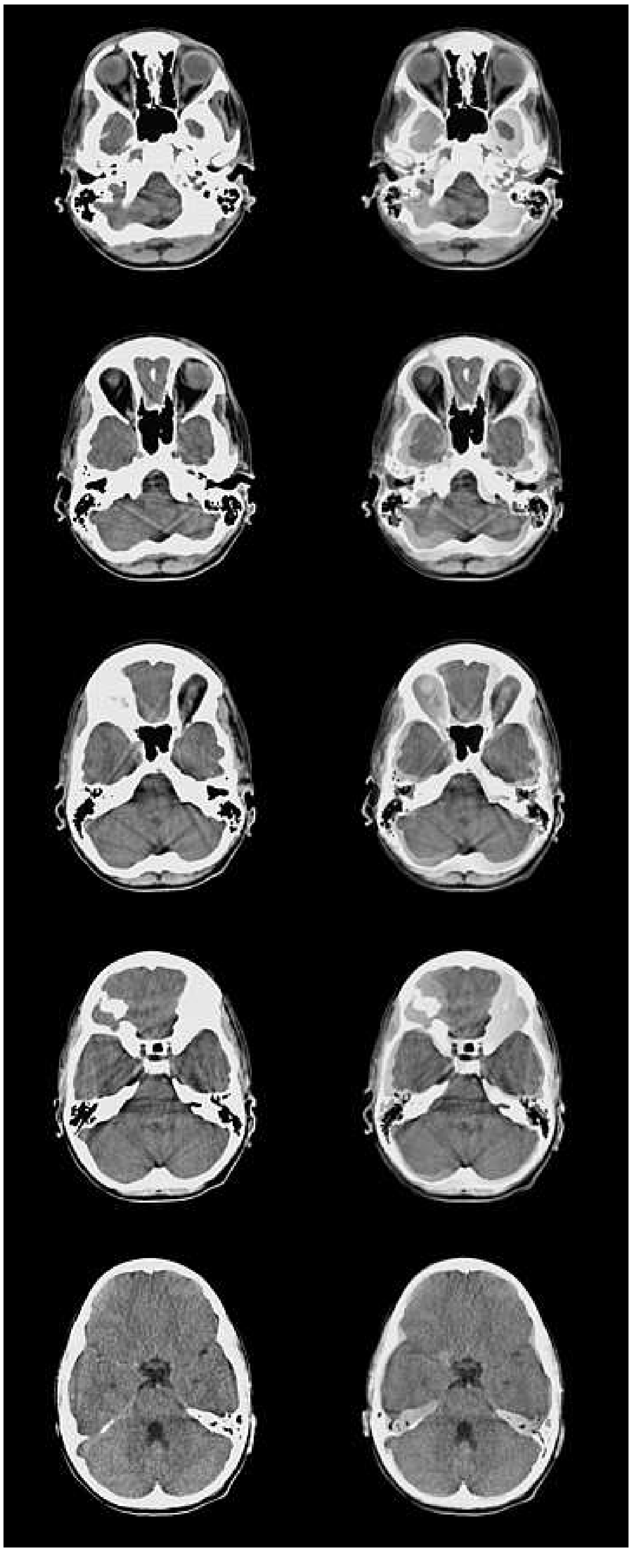

Figure 17: Left: The input axial slices; Right: corresponding resliced axial slices with corrected yaw and roll angles. Notice the ones on the right are more symmetric.

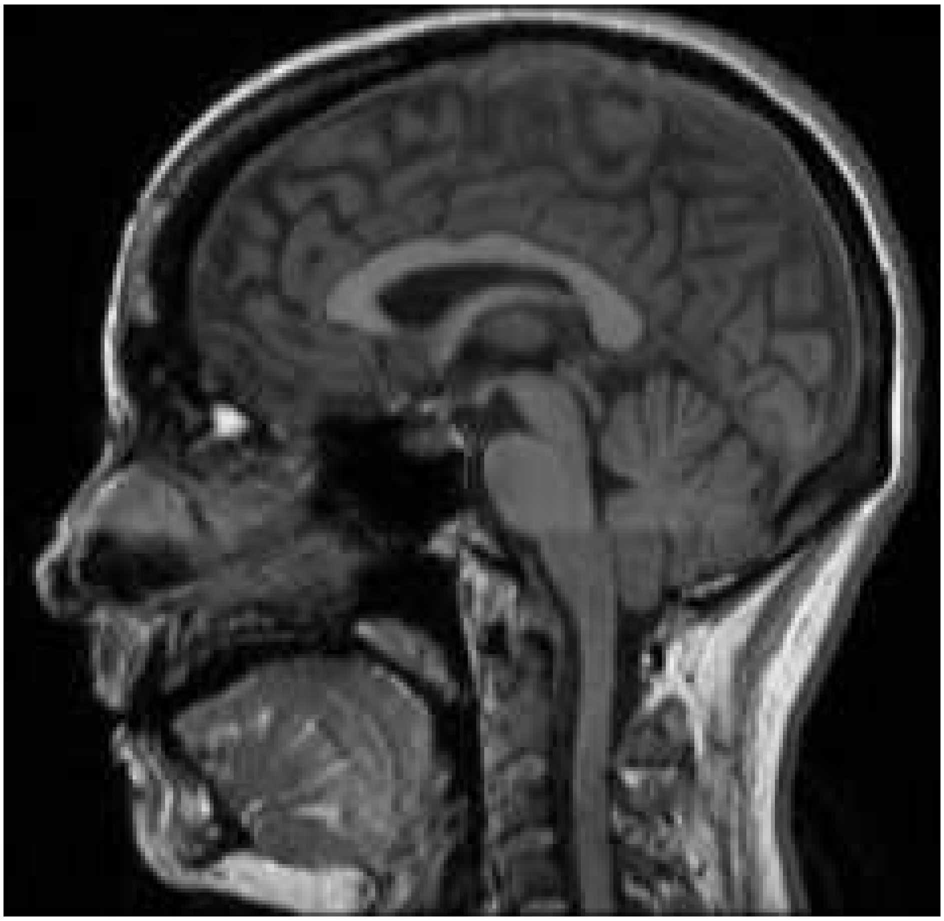

Figure 18: The mid-sagittal plane automatically extracted from the MR data set. The detected yaw is 1.25 degrees and the detected roll angle is -1.75 degrees.

3 Lesion and Mass Effect Detection

As one application of the result from the previous symmetry axes extracting algorithm, we sketch the use of the estimated symmetry axis on each slice to detect bilateral asymmetries that may signal the presence of lesions and mass effect. The steps taken are

1. Rotate and crop the slice so the symmetry axis is vertical and centered in the image, call this image S (Figure 19a).
2. Extract canny edges [2] from S_i and link them into chains [11].
3. Flip image S about its vertical center line to get $ref_V(S)$.
4. Subtract image S from the flipped image $ref_V(S))$ and take the absolute value of the difference, $D = abs(S - ref_V(S))$ (Figure 19c)
5. Extract canny edges of D and link them into chains (Figure 19d).
6. Match chains from S with chains from D using the Hausdorff metric [5]. Identify only those that match in both directions to less than a threshold. The result is shown in Figure 20, where the lesion and the enlarged ventricle are contoured.

Using these contours we are able to build 3D surface models for the lesions detected.

4 Discussion and Conclusions

We have shown a simple yet effective algorithm that can automatically locate the mid-sagittal plane given a set of neuroradiology images. The algorithm works on brain slices from both normal and pathological brains, as well as on images with cluttered background. The algorithm and its application to lesion detection have been implemented on an SGI Indy 5000 using Matlab together with some user-defined C routines.

Though our reasonings in Section 2.5 are precise and justified, when calculating roll (yaw) angles from input axial (coronal) slices, the results are sometimes less than ideal. Figure 21 shows the plot of calculated roll angles given a set of MR axial slices with varied roll angles. The output of the algorithm on roll angle variations is consistent with the input data in a linear fashion, but it tends to underestimate the roll angle, particularly for larger rolls. This is because the actual medial line of the brain is shifted so far off from the symmetry axis of the whole image (Figure 22). To locate the exact $trans_i$ in these images, one would need to use more sophisticated procedures looking

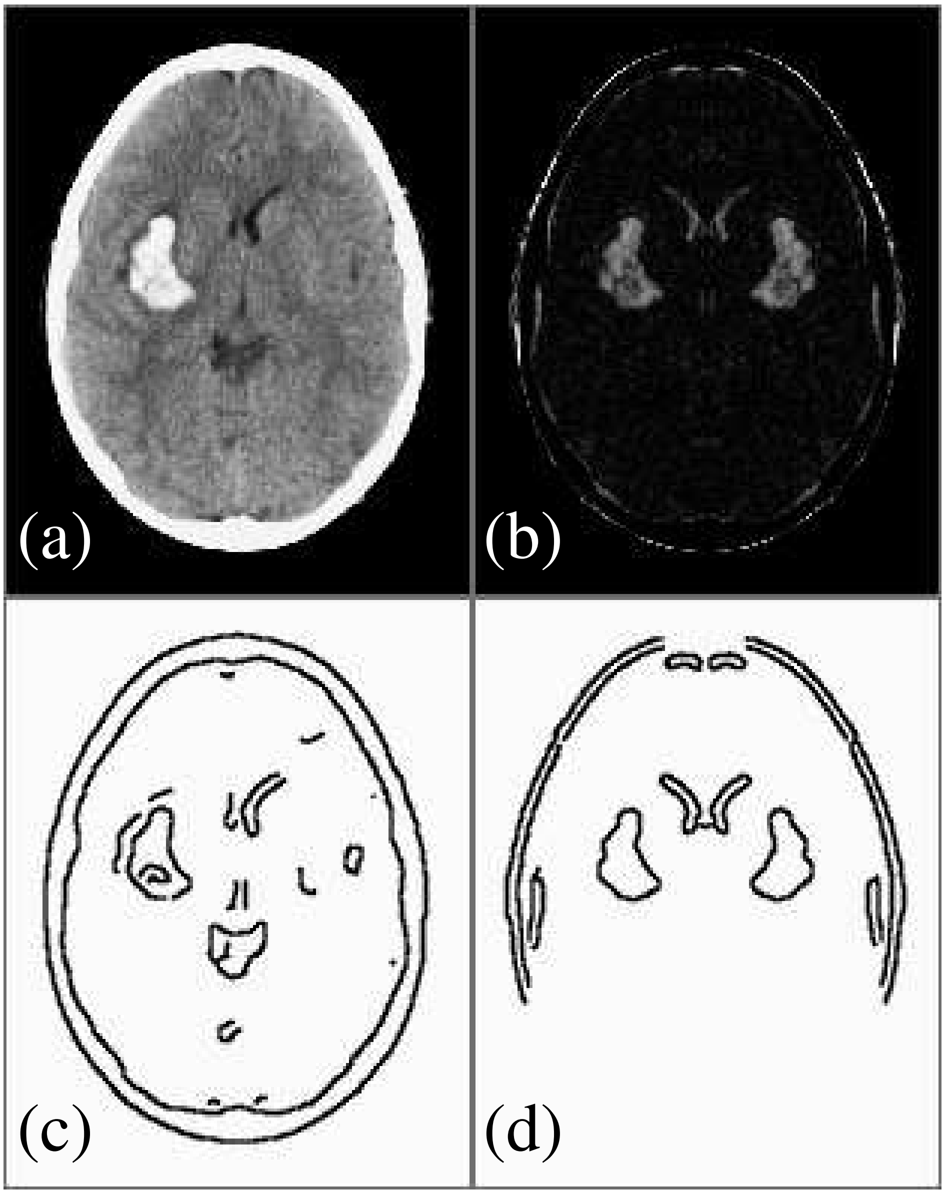

Figure 19: Lesions and mass effect are detected by matching curves extracted from the original head image and the absolute difference of the head image subtracted from a reflected version.

Figure 20: Results of lesion and mass effect detection. Background figure has been brightened to make curves more visible.

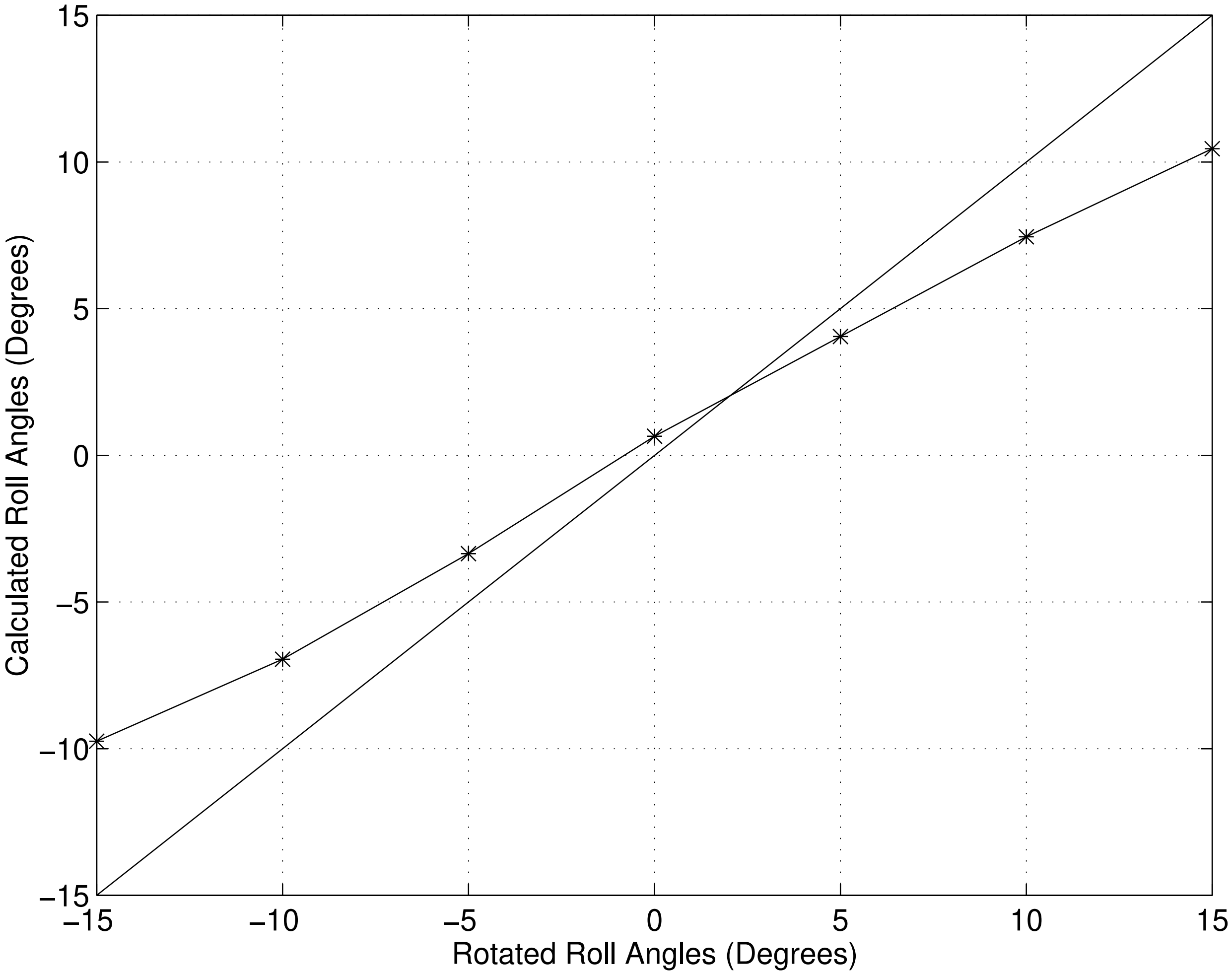

Figure 21: Actual vs calculated roll angles. Solid line: ideal result. The line with *s: calculated result.

for specific medial anatomic features, such as the falx (a straight line, white on CTs, appearing on higher cuts), or pons (in lower cuts) etc.; or one can use active contour algorithms (snakes) with the found symmetry axis at the starting position for the mid-line. We are exploring both of these approaches. Alternatively, we have applied our algorithm to the coronal slices to estimate the roll angles and achieved accurate results as shown in Section 2.5. This fact also implies that the

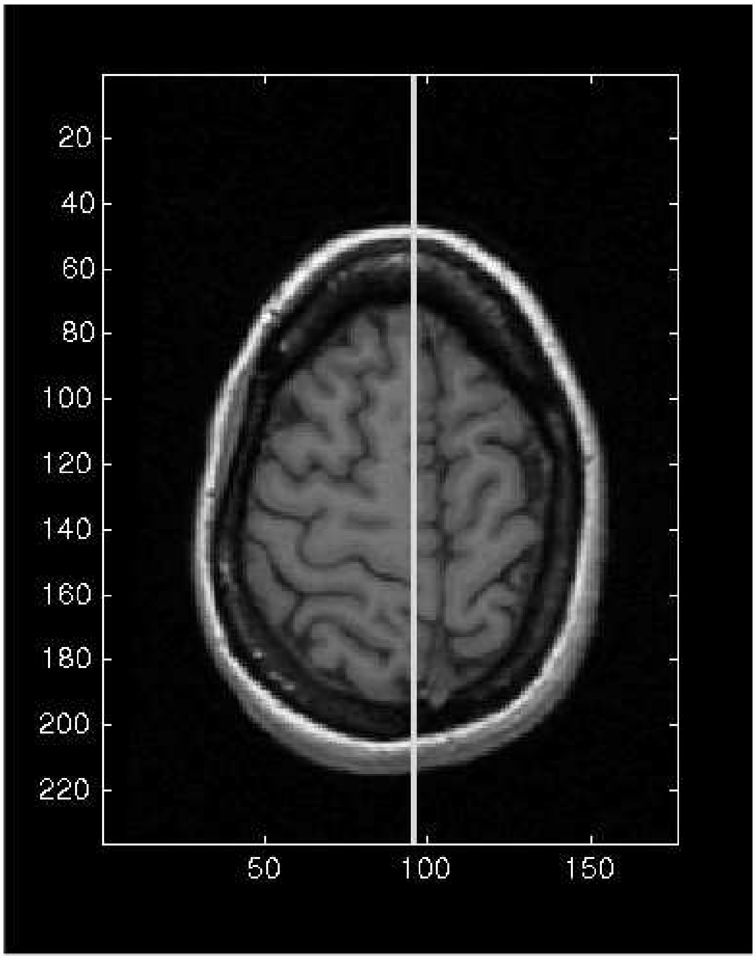

Figure 22: The symmetry axis extracted from a brain slice with a large roll angle (10 degrees in this case) is pulled towards the medial line which separates the two hemispheres of the brain, but not far enough to overlap with the medial line.

symmetry axis can not be determined by the silhouette of an axial or coronal brain slice alone, but must be determined with respect to the internal structure of the brain.

Using this algorithm one can estimate two degrees of rotational freedom (yaw and roll) as well as one degree of translation (along the X_0 axis), that is why we can accurately locate the mid-sagital plane in the brain. There are still three degrees of pose freedom left (it is not an accident that that the leftover degrees of freedom form the symmetry group of the plane [6]). No information about pitch angle ω can be determined from the orientation of the symmetry plane. In order to bring the working coordinate system into a complete alignment with the ideal head coordinate system, these three degrees of freedom can be determined using domain knowledge other than symmetry, such as locating anatomical landmarks like the *anterior commissure* and *posterior commissure* [10], or using more sophisticated methods such as reported in [3, 4]. The fact that this algorithm does not use any built-in knowledge about the human brain, other than its bilateral symmetry, suggests that it may have other applications in areas outside of neuroradiology, for example on images involving approximate bilateral, rotational and translational symmetries such as those used in [7].

The results of this algorithm can be used to correct for rotational errors in both the yaw and roll directions with an accuracy of less than one degree (regardless of the amount of the rotational errors in the input data), establish a common center plane (the mid-sagittal plane) for registration and comparison of different sets of brain scans, and set the center line for detecting mass effect in each brain slice as we have shown in Section 3. This fast symmetry detection algorithm can also be used to screen out relatively symmetrical images as *normal* ones, and asymmetrical ones as candidates of *abnormal* brain images. This is just the first step towards our long term goal to build a true content-based medical image understanding system that can intelligently store, retrieve and compare medical images.

Our current work includes an extensive testing of the lesion detection algorithm; deformable registration of the mid-sagittal planes between patients' data and a brain atlas; and determination of the anatomical location of a detected lesion.

Acknowledgements

Helpful comments were given by Chuck Thorpe, Takeo Kanade, Andrew Johnson and David Simon. Thanks to Cathy Poole and the Radiology Department of AGH for providing the CT images, and thanks to Mei Chen and Aveek Datta of CMU for their help in getting the raw image data. Thanks the CNSoftware Inc. for providing the MR image set as part of the testing data.

References

[1] P. Allain, J.M. Travère, J.C. Baron, and D. Bloyet. *Quantification of Brain Function. Tracer Kinetics and Image Analysis in Brain PET: Accurate PET positioning with reference to MRI and neuroanatomical data bases*, pages 401,408. Elsevier Science Publishers, B.V., 1993.

[2] John Canny. A computational approach to edge detection. *IEEE Pattern Analysis and Machine Intelligence*, 8(6):679–698, 1986.

[3] C. Davatzikos. Nonlinear registraion of brain images using deformable models. In *Proceedings of the workshop on Mathematical Methods in Biomedical Image Analysis*, pages 94,103. IEEE Computer Society, June 1996.

[4] J. Feldmar, G. Malandain, J. Declerck, and N. Ayache. Extension of the icp algorithm to non-rigid intensity-based registration of 3d volumes. In *Proceedings of the workshop on Mathematical Methods in Biomedical Image Analysis*, pages 84,93. IEEE Computer Society, June 1996.

[5] D. Huttenlocher, G. , Klanderman, and W. , Rucklidge. Comparing images using the hausdorff distance. *IEEE trans. on Pattern Analysis and machine Intelligence*, 15(9):850,863, 1993.

[6] Y. Liu and R. Popplestone. A Group Theoretical Formalization of Surface Contact. *International Journal of Robotics Research*, 13(2):148 – 161, April 1994.

[7] T. Masuda, K. Yamamoto, and H. Yamada. Detection of partial symmetry using correlation with rotated-reflected images. *Pattern Recognition*, 26(8):1245,1253, 1993.

[8] A. Rosenfeld and A.C. Kak. *Digital Picture Processing*. Academic Press, New York, 1976.

[9] John C. Russ. *The Image Processing Handbook*. CRC Press, Boca Raton, Ann Arbor, London, Tokyo, 1992.

[10] J. Talairach and P. Tournoux. *Co-Planar Steriotaxic Atlas of the Human Brain*. Thieme Medical Publishers, 1988.

[11] S. Venkatesh and P.L. Rosin. Dynamic threshold determination by local and global edge evaluation. *Graphical Models and Image Processing*, 75(2):146,160, 1995.